Carcinogenesis, 2024, **XX**, 1–12
https://doi.org/10.1093/carcin/bgae047
Advance access publication 25 July 2024
Original Article

OXFORD

Original Article

Enhancing carboplatin sensitivity in ovarian cancer cells by blocking the mercapturic acid pathway transporter

B. Madhu Krishna[1,‡], Sravani K. Ramisetty[1,‡], Pankaj Garg[2], Atish Mohanty[1], Edward Wang[1], David Horne[3], Sanjay Awasthi[4], Prakash Kulkarni[1], Ravi Salgia[1], Sharad S. Singhal[1,*]

[1]Department of Medical Oncology, Beckman Research Institute, City of Hope Comprehensive Cancer Center and National Medical Center, Duarte, CA 91010, United States
[2]Department of Chemistry, GLA University, Mathura, Uttar Pradesh 281406, India
[3]Department of Molecular Medicine, Beckman Research Institute, City of Hope Comprehensive Cancer Center and National Medical Center, Duarte, CA 91010, United States
[4]Cayman Health, CTMH Doctors Hospital in Cayman Islands, George Town, Grand Cayman

[‡]These authors contributed equally to this work and should be considered co-first authors.
[*]Corresponding author. Department of Medical Oncology, Beckman Research Institute, City of Hope Comprehensive Cancer Center and National Medical Center, Duarte, CA 91010, USA. E-mail: ssinghal@coh.org

Abstract

Ral-binding/interacting protein (RLIP) acts as a transporter that responds to stress and provides protection, specifically against glutathione–electrophile conjugates and xenobiotic toxins. Its increased presence in malignant cells, especially in cancer, emphasizes its crucial antiapoptotic function. This is achieved by selectively regulating the cellular levels of proapoptotic oxidized lipid byproducts. Suppressing the progression of tumors in human xenografts can be achieved by effectively inhibiting RLIP, a transporter in the mercapturic acid pathway, without involving chemotherapy. Utilizing ovarian cancer (OC) cell lines (MDAH2774, OVCAR4, and OVCAR8), we observed that agents targeting RLIP, such as RLIP antisense and RLIP antibodies, not only substantially impeded the viability of OC cells but also remarkably increased their sensitivity to carboplatin. To delve further into the cytotoxic synergy between RLIP antisense, RLIP antibodies, and carboplatin, we conducted investigations in both cell culture and xenografts of OC cells. The outcomes revealed that RLIP depletion via phosphorothioate antisense led to rapid and sustained remissions in established subcutaneous human ovary xenografts. Furthermore, RLIP inhibition by RLIP antibodies exhibited comparable efficacy to antisense and enhanced the effectiveness of carboplatin in MDAH2774 OC xenografts. These investigations underscore RLIP as a central carrier crucial for supporting the survival of cancer cells, positioning it as a suitable focus for cancer treatment.

Graphical Abstract

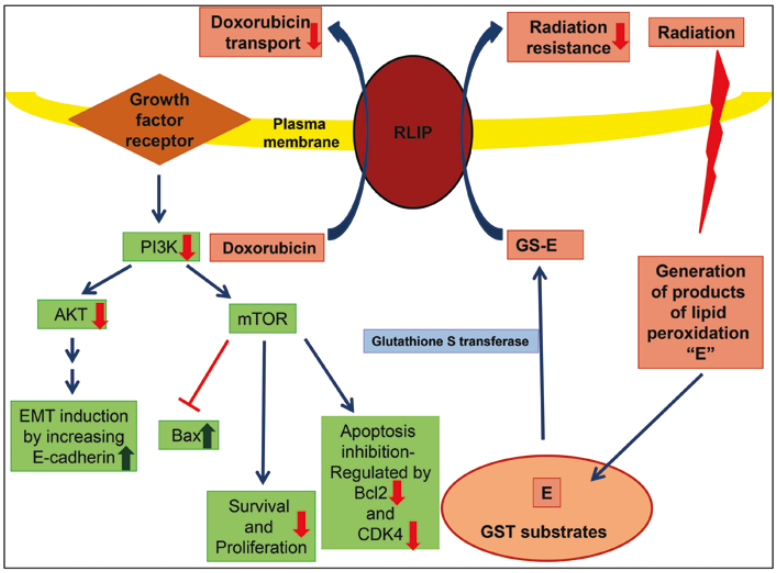

Keywords: RLIP; mercapturic acid pathway; chemotherapeutics; tumor xenografts; glutathione conjugates

Received: April 25 2024; revised: June 23 2024; accepted: July 19 2024

1. Introduction

Ovarian cancer (OC) stands out as exceptionally aggressive and the most malignant gynecologic neoplasm affecting women. Approximately 90% of all OCs are ovarian epithelial cancers, representing the leading cause of death among them [1]. The challenge of platinum resistance significantly impedes OC treatment and correlates with unfavorable clinical outcomes. Intra-tumor heterogeneity plays a pivotal role in the development of chemoresistance. Presently, the standard treatment for OC involves chemotherapy utilizing platinum drugs (cisplatin or carboplatin) combined with paclitaxel. This approach is adopted because platinum drugs and paclitaxel activate diverse apoptosis signaling pathways in OC. Platinum drugs induce cell apoptosis by crosslinking DNA, while paclitaxel halts the cell cycle at the G2/M phase through binding to the β-tubulin subunit of microtubules. However, clinical outcomes are hindered by the distinct pharmacokinetics and bio-distributions of platinum drugs and paclitaxel, attributed to their differing lipophilicities [2, 3]. Despite initial positive responses to surgery and chemotherapy, the majority of tumors eventually develop drug resistance, leading to relapse [4]. Consequently, most patients succumb to the disease, underscoring the imperative need for innovative treatments to enhance existing therapeutic options. The activation of the phosphatidylinositol 3' –kinase/Protein kinase B (PI3K/Akt) signaling pathway is widely acknowledged to contribute to the pathogenesis of ovarian carcinomas [5, 6].

Ral-binding/interacting protein (RLIP) functions as a protective protein against stress, hindering the accumulation of detrimental metabolites caused by lipid oxidation products. Its mechanism involves transporting glutathione–electrophile conjugates (GS–E) out of cells in an adenosine triphosphate (ATP)-dependent manner, thereby counteracting apoptosis [7–12]. Studies on mice with homozygous knockout of RLIP reveal a significant 2- to 7-fold increase in the buildup of lipid hydroperoxides, aldehydes, and alkenals [12]. This aligns with a considerable reduction of more than 80% in the overall activity of transporting GS–E and anthracycline. Such a downturn leads to a noteworthy amplification in sensitivity to xenobiotic poisons, encompassing chemotherapy drugs derived from natural products directly carried by RLIP, in addition to metabolized alkylating agents and platinum coordinates to form GS–E. Surveys utilizing gene-expression arrays have identified increased RLIP expression in diverse cancerous cells. Apoptosis is triggered in cultured cells from a spectrum of human hematological and solid malignancies, including OC, lung cancer, prostate cancer, colon cancer, melanoma, and lymphoma [13].

This finding naturally prompted an inquiry into the applicability of these noted phenomena to human malignancies and whether enhancing or obstructing RLIP might enhance the effectiveness of cytotoxic chemotherapy. Ongoing investigations tackle these questions through trials conducted in cultures of cells and xenografts in nude mice, incorporating cell lines derived from human OC. Here, in OC xenograft models, we explore the potential outcome of inducing regression in cancer through RLIP reduction using antisense techniques. Additionally, in the OC model, both in cell cultures and xenografts, we explore the potential of enhancing carboplatin's efficacy by inhibiting RLIP with RLIP antibodies, suppressing PI3K/Akt signaling. We selected this specific chemotherapy combination for its acknowledged synergistic properties and because it stands out as the initial combination chemotherapy proven to prolong survival in an adjuvant setting.

2. Materials and methods

2.1. Materials

Carboplatin (cat # S1215) was supplied by Selleck Chemicals LLC (Houston, TX, Sylvanfield Drive). Antibodies for RLIP (cat # sc-28575), cyclin B1 (cat # sc-595), Bax (cat # sc-493), CD31 (cat # sc-71872), and Ki67 (cat # sc-23900) from Santa-Cruz Biotechnology (Columbus, OH), β-actin (cat # bs-0061R) from Bioss Antibodies (Woburn, MA), and pAkt (S^{473}) (cat # 9018P), CDK4 (cat # 12790), Bcl2 (cat # 2872S), E-cadherin (cat # 4065P), pPI3K (Y^{458}) (cat # 4228P), cleaved PARP (cat # 9541), and vimentin (cat # 5741) from Cell Signalling Technologies (Danvers, MA) were procured. Cambrex Bio-Science (Walkersville, MD) procured the serum-free medium (K-SFM), Keratinocyte, and EGM-2 bullet kit medium. GIBCO-BRL, Grand-Island, New York, supplied Dulbecco's Modified Eagle Medium (DMEM) medium, phosphate-buffered saline (PBS), RPMI-1640, fetal bovine serum (FBS), penicillin/streptomycin (P/S) solution, trypan blue, and trypsin–EDTA. Reagents for sodium dodecyl sulfate–polyacrylamide gel electrophoresis (SDS–PAGE) were provided by Bio-Rad Laboratories (Hercules, CA). MTT (3-(4,5-dimethylthiazol-2-yl)-2,5-diphenyltetrazolium bromide) (cat # M2128) was supplied by Sigma–Aldrich (St. Louis, MO), and the TUNEL Fluorescence Apoptosis Detection kit (cat # G3250) was purchased from Promega (Madison, WI). Anti-mouse peroxidase conjugates secondary antibodies (cat # 7076S) and horseradish peroxidase (HRP)-conjugated anti-rabbit antibodies (cat # 7074S) were furnished by Cell Signaling Technologies (Danvers, MA). The sources for the previously mentioned reagents [14] remained consistent. The cell invasion assay kit was acquired from Cell Biolabs (San Diego, CA). Dojindo Molecular Technologies (Rockville, MD) provided the cell counting kit-8 (CCK-8) for the cell viability assay. The Universal Mycoplasma Detection Kit was obtained from The American Type Culture Collection (ATCC, Manassas, VA).

2.2. Cell lines and cultures

Dr Edward Wang, from the Department of Medical Oncology at City of Hope, National Medical Center, and Beckman Research Institute, Duarte, CA, generously supplied the human OC cell lines (OVCAR4, OVCAR8, and MDAH2774). Human umbilical vascular endothelial cells (HUVECs) and human aorta vascular smooth muscle cells (HAVSMCs) were kindly provided by Dr Fiemu Nwariaku from the University of Texas Southwestern Medical Center in Dallas, TX. Cultured in the appropriate medium: OC cells (OVCAR4, MDAH2774, and OVCAR8) were maintained in RPMI-1640 at 37°C in a humidified atmosphere with 5% CO_2. The mediums used were the EGM-2 bullet kit for HUVEC and DMEM for HAVSMC. These mediums were prepared by supplementing with 1% (v/v) P/S solution, 10% (v/v) heat-inactivated FBS, 10 mmol/l (4-(2-hydroxyethyl)-1-piperazineethanesulphonic acid) (HEPES), 2 mmol/l L-glutamine, 1 mmol/l sodium pyruvate, 1.5 g/l sodium bicarbonate, and 4.5 g/l glucose. The authenticity of cell lines was verified by the City of Hope Integrative Genomics Core, Duarte, CA, using 15 different human short tandem repeats. Regular screening for mycoplasma occurred every 3 months across all cell types.

2.3. RLIP phosphorothioate antisense preparation

Desalted phosphorothioate DNA, chemically synthesized, was provided by Biosynthesis (Lewisville, TX). For control purposes, phosphorothioate DNA featuring a 21-nucleotide scrambling was employed [13].

2.4. Cell viability assay

Assessing cellular viability included MTT assays to explore the impact of RLIP inhibition and depletion on the survival of OC cells (MDAH2774, OVCAR4, and OVCAR8) and normal cells (HUVEC and HAVSMC). To measure cell density, viable cells resistant to trypan blue staining were examined using a hemocytometer. Initiated with a seeding density of 5000 cells per well in 96-well microtiter plates with a flat bottom, the cells experienced a 24-h treatment. This involved RLIP antibodies (40 μg/ml) or transfection with RLIP antisense oligonucleotides (10 μg/ml) using Maxfect Transfection Reagent (MoleculA), adhering to the manufacturer's specified protocol. After a 24-h incubation, eight replicate wells received 40 μl aliquots of carboplatin, ranging from 1 to 100 μM, to ascertain the drug's concentration that is required for 50% inhibition in vitro (IC_{50}), defined as the concentration leading to a 50% reduction in formazan. Subsequent to an additional 48-h incubation, 10 μl of MTT (5 mg/ml) was introduced to each well, and the plates were left to incubate for 2 h at 37°C. Following this incubation, a prompt PBS wash was performed, and the supernatant was aspirated. To assess well absorbance, formazan crystals were dissolved in 100 μl of dimethyl sulfoxide (DMSO) by gently shaking for 2 h at room temperature. A Microplate XMark™ spectrophotometer (Bio-Rad, Hercules, CA) was employed for this purpose. Cell survival percentage was calculated using the formula (absorbance treatment/absorbance control) × 100, after background correction of absorbance. The table presented consolidates data from three independent experiments, each with four replicate wells per treatment, including mean and standard deviation (SD). Western blot analysis using RLIP antisense was conducted to validate the extent of RLIP depletion.

2.5. Chou–Talalay median effect analysis of synergy

The assessment of synergy, following the Chou–Talalay method [15], involves determining IC_{50} values individually and in combination for each drug. Utilizing the Calcusyn software package, an analysis is carried out, employing an algorithm that takes into account cytotoxicity and dose–effect curves for individual chemotherapy drugs and antibodies. Involving two or three drugs, synergy assessment calculates the combination index (CI) from the isobologram equation. Indicating synergy, additivity, and antagonism with CI values less than 1, equal to 1, and greater than 1, respectively.

2.6. Detection of RLIP protein expression in normal and OC cell lines

Cell extraction was performed using trypsinization for both OC cell lines (MDAH2774, OVCAR4, and OVCAR8) and normal cells (HAVSMC and HUVEC) to detect RLIP protein expression. SDS lysis buffer (Cell Signalling Technologies) with protease and phosphatase inhibitors (Roche, Indianapolis, IN) was used for cell lysis. The lysis process included a sonication step to separate cell membranes from the pellets. Electrophoresis of 100 μg total protein was carried out on 12.5% SDS–polyacrylamide gels at 200 V for 1 h. Protein transfer to nitrocellulose membranes was performed at 100 V for 70 min at 4°C. The blots were incubated overnight at 4°C with primary RLIP antibodies (1:1000). On the following day, the blots were subjected to a rinse with 1× TBS (Tris-buffered saline)-Tween (0.1%), followed by a 2-h incubation at room temperature with secondary antibodies (HRP conjugated, 1:5000). Thermo Fisher Scientific's Super Signal West Pico Chemiluminescent Substrate was utilized for blot analysis, and the images were captured using Alpha Innotech's Multi-Image Light Cabinet. RLIP protein expression levels were normalized against β-actin expression levels. The western blot analysis was performed in triplicate, and the presented images illustrate representative replicates.

2.7. Colony formation assay

Undergoing treatment, cells (0.1×10^6 cells/500 μl) were exposed to both scrambled antisense and RLIP antisense (final concentration of 10 μg/ml) for 48 h. Subsequently, independent incubation took place in 60 mm Petri plates, with each plate containing a total medium volume of 4 ml, using 50 and 100 μl aliquots. After 7 days, the adherent colonies were preserved and stained for 30 min with 0.5% methylene blue. Quantification was performed utilizing an Innotech Alpha Imager HP [16].

2.8. Cell migration assay

Evaluating the impact of RLIP antisense on the migratory behavior of MDAH2774 and OVCAR8 OC cells involved the utilization of a wound healing assay. Seeding cells into 6-well dishes, they were permitted to attain around 90% confluence. A wound was generated across the cell monolayer using a sterilized 10 μl pipette tip. After the removal of cellular debris with PBS, each well was supplied with serum-free medium, and cells were subjected to treatment with either scrambled or RLIP antisense (final concentration of 10 μg/ml). Immediate microscopic images of the formed gap were captured, along with subsequent images after 12 and 24 h. The assessment of cell migration capacity involved measuring the width of the wound in the cell monolayer at 0, 12, and 24 h post-scraping. The data presented depict the mean and SD derived from three distinct experiments.

2.9. Cell invasion assay

Examining the *in vitro* impact of RLIP antisense on the migratory patterns of MDAH2774 OC cells involved in employing the Transwell Boyden chamber. To elaborate, the upper chamber of 24-well Transwell plates held MDAH2774 cells (0.5×10^6 cells/well) suspended in a serum-free medium. Treatment with either scrambled or RLIP antisense (final concentration of 10 μg/ml) was conducted over a 24-h period. In the lower chamber, DMEM medium supplemented with 10% FBS was introduced. Incubation took place in a humidified atmosphere with 95% air and 5% CO_2 at 37°C. At specific intervals, nonmigratory cells within the insert were eliminated by wiping with a PBS-soaked cotton swab, while migratory cells attached to the underside of the insert were fixed using 4% paraformaldehyde for 15 min. Following that, these cells experienced permeabilization using 0.2% Triton X-100 in PBS and were then stained with 0.2% crystal violet for 10 min at room temperature. Capturing images of migrating cells occurred in five randomly chosen fields within the insert, utilizing a light microscope (200×). Subsequently, the stained inserts were gently rinsed with water, moved to an empty well, extracted with 200 μl of

extraction buffer, and left to incubate for 10 min on an orbital shaker. The determination of the number of invaded cells per membrane was achieved by measuring absorbance at 560 nm in a plate reader. This absorbance value served to quantify the percentage of invasive cells in RLIP antisense-treated cells in comparison to those treated with scrambled antisense. The experiments were performed in triplicate.

2.10. *In vivo* xenograft studies

To measure the potential efficacy of an antineoplastic agent in preclinical assessment, the pivotal step involves evaluating its performance in an animal model. Female mice, specifically the Hsd: Athymic nude *nu/nu* strain, were procured from The Jackson Laboratory, Bar Harbor, ME. All experiments involving animals followed a protocol approved by the Institutional Animal Care and Use Committee (IACUC). A grouping of forty 10-week-old female mice was performed, dividing them into eight groups, each comprising five animals. These groups underwent treatments with preimmune serum, scrambled antisense, RLIP antibodies, RLIP antisense, carboplatin, and various combinations, as outlined in Figs 3 and 4. After acclimating for a week, all animals underwent subcutaneous injection in one flank with 1×10^6 MDAH2774 OC cell suspensions in 100 µl of PBS. Treatment initiation occurred 13 days postimplantation when the tumor became perceptible (surpassing a surface area of ~35 mm^2). The treatment regimen included RLIP antibodies (4 mg/kg b.w.), RLIP antisense (4 mg/kg b.w.), carboplatin (20 mg/kg b.w.), RLIP antisense + carboplatin, RLIP antibodies + carboplatin, and RLIP antisense + RLIP antibodies + carboplatin, all administered in 100 µl PBS. Control groups received treatment with preimmune serum or scrambled antisense (4 mg/kg b.w.). Over the course of 8 weeks, intraperitoneal treatments were administered weekly, and a constant watch for signs of tumor development in the animals was maintained. Tumor dimensions were measured with calipers in two dimensions, and both body weights and tumor dimensions were recorded. Animal photographs were taken on days 1, 7, 14, 21, 28, 35, 42, 49, and 56 after the initiation of treatment. Upon completion of the experiment, mice were humanely euthanized through cervical dislocation and CO_2 asphyxiation. Additionally, on day 56, images of the tumors were captured. Tumor weights were compared between groups using an unpaired Student's *t*-test. For subsequent molecular investigations, such as western blot analysis, tumor tissues were either snap-frozen in liquid nitrogen or treated in a 10% buffered formaldehyde solution and paraffin-embedded for immuno-staining. Immunoblotting: tumor tissue protein lysates were obtained through the utilization of radio-immunoprecipitation assay (RIPA) buffer, inclusive of proteinase and phosphatase inhibitors. The BCA protein assay kit (Pierce Biotechnology, Rockford, IL) was employed to ascertain protein concentrations. Loading and separation of lysates (100 µg) occurred on SDS–PAGE, succeeded by the transfer to a nitrocellulose membrane. After blocking the membrane for 1 h at room temperature with 5% nonfat dry milk in TBS with Tween 20 (TBST), an overnight incubation with primary antibodies at 4°C ensued. Subsequent washes with TBST were performed, and the membranes underwent a 2-h incubation at room temperature with HRP-conjugated secondary antibodies. Visualization of signals was accomplished using an enhanced chemiluminescence detection kit.

2.11. Immunohistochemical analysis

Mice in all eight treatment categories were subjected to diverse treatments, such as control scrambled antisense, RLIP antisense, preimmune serum, RLIP antibodies, carboplatin, or combinations thereof. Subsequently, tumor tissues were extracted from mice in each group, fixed in buffered formalin for 24 h, embedded in paraffin, sliced into 5-µm-thick sections, and affixed to slides coated with poly-L-lysine. Deparaffinization and rehydration of tissue sections, fixed in buffered formalin and embedded in paraffin, were achieved by sequentially passing through xylene and graded ethanol solutions. Following this, the slides were subjected to treatment with 3% hydrogen peroxide with 0.03% sodium azide in PBS for 10 min. Microwave antigen retrieval was then performed at 100°C for 10 min in DAKO Target Retrieval Solution (DAKO Corporation, Carpinteria, CA) using an H2800 Microwave Processor (Energy Beam Sciences, Agawam, MA). Tissue sections were stained using hematoxylin and eosin (H&E). Antibodies directed against RLIP, CD31, E-cadherin, Ki67, and vimentin were detected utilizing a universal avidin/biotin complex detection kit from Vector. Sections displaying immunoreactivity exhibited a dark brown stain, while nonreactive sections showed background staining. Photomicrographs were captured using a 40× magnification Olympus DP72 microscope. The degree of antigen staining was quantified through the DP2-BSW program and digital image processing.

2.12. Statistical analysis

The data are portrayed as the mean ± SD obtained from a minimum of three independent experiments, unless explicitly mentioned otherwise. A scatter plot was employed to illustrate variations in both body weight and tumor size over the course of the experiment. Statistical significance in differences between the control and treatment groups was evaluated using paired *t*-tests or two-way analysis of variance. A *P*-value of ≤.05 was considered statistically significant. All statistical tests conducted were two-sided, and the error bars represent standard error from triplicates.

2.13. Ethics statement

No human participation was involved in the study. The animal research adhered to the City of Hope Animal Care and Ethics Committee's IACUC procedure # 22011 and conformed to ethical standards. Mice manifesting signs of distress, pain, or suffering due to their tumor burden were compassionately and humanely euthanized.

3. Results

3.1. Expression levels of RLIP in OC cells

Western blot analyses were conducted on membrane protein extracts from both human normal and OC cells. The results displayed a significant rise in RLIP abundance in OC cells compared with their normal counterparts (Fig. 1A). This observation implies that RLIP might be a potential candidate for inhibiting the proliferation of OC cells. Table 1 provides a breakdown of RLIP protein levels, illustrating the total amount of crude membrane proteins obtained from 10^8 cells during the logarithmic growth phase. RLIP protein content was identified to be around ~11 ± 2 µg/10^8 normal cells and ~53 ± 5 µg/10^8 OC cells, making up 0.19% and 0.72%,

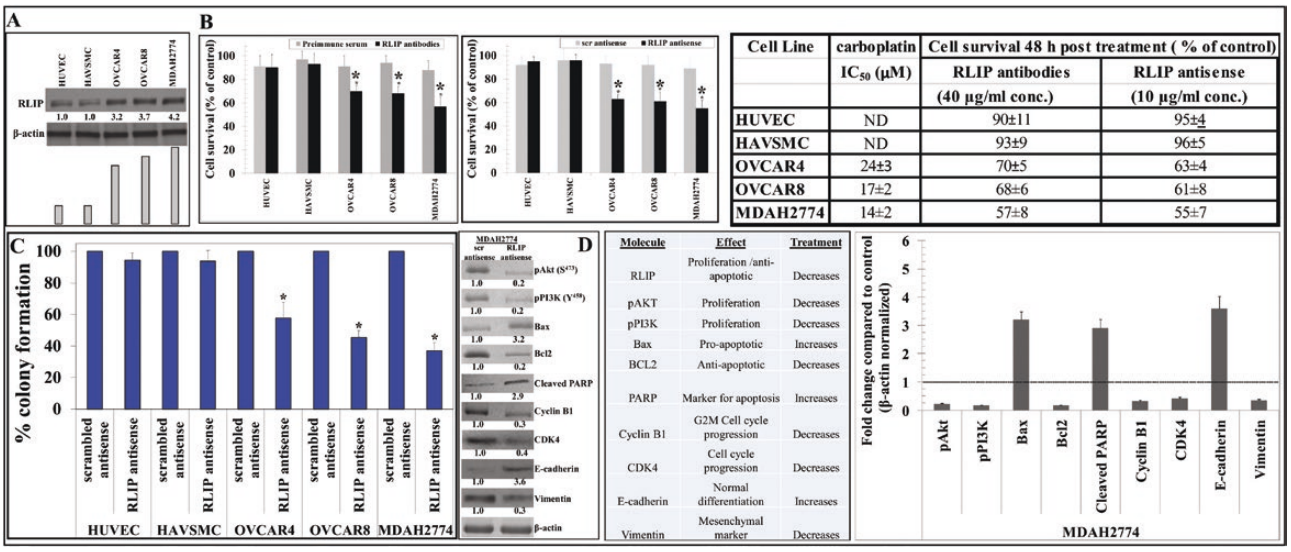

Cell Line	carboplatin IC_{50} (μM)	Cell survival 48 h post treatment (% of control)	
		RLIP antibodies (40 μg/ml conc.)	RLIP antisense (10 μg/ml conc.)
HUVEC	ND	90±11	95±4
HAVSMC	ND	93±9	96±5
OVCAR4	24±3	70±5	63±4
OVCAR8	17±2	68±6	61±8
MDAH2774	14±2	57±8	55±7

Figure 1 Comparison of RLIP levels between OC cells (MDAH2774, OVCAR4, and OVCAR8) and nonmalignant cells (HUVEC and HAVSMC). Crude membrane fractions containing 100 μg protein were subjected to SDS–PAGE and western blotting. The RLIP protein band's intensity was quantified using scanning densitometry with Innotech Alpha Imager HP. β-Actin served as the internal control (panel A). The impact of RLIP antisense, RLIP antibodies, and carboplatin on both normal and OC cells was assessed. Ovarian cell lines underwent carboplatin treatment (0–100 μM) for 48 h. Inhibition or depletion of RLIP exhibited selective decreases in the survival of malignant OC cells compared with normal cells. RLIP function was inhibited by RLIP antibodies, and RLIP expression was depleted by RLIP antisense using Maxfect Transfection Reagent (Molecula) as per the manufacturer's instructions. Cell survival was evaluated through the MTT cytotoxicity assay 48-h post-treatment. In a 96-well plate, RLIP antibodies were used at a final concentration of 40 μg/ml, and RLIP antisense was at 10 μg/ml. The table presents the IC_{50} values (μM) of carboplatin and the percentage of cell survival after RLIP antibodies and RLIP antisense treatment. Values represent mean ± SD from three separate determinations with four replicates ($n = 12$). "ND" indicates not detected. Statistical significance was determined by Student's *t*-test (*$P < .02$) compared with respective controls (panel B). Colony-forming efficiency in OC cells and nonmalignant cells post-antisense treatment was assessed by methylene blue staining, and colony counting was conducted using Innotech Alpha Imager HP (*$P < .04$) compared with respective controls (panel C). The impact of RLIP antisense on oncogenic signaling in MDAH2774 cells was investigated. Treatment with 10 μg/ml of RLIP antisense for 24 h led to the inhibition of the PI3K/Akt pathway. Immune blotting was performed for Bax, pAkt, Bcl2, cyclin B1, cleaved PARP, CDK4, E-cadherin, pPI3K, and vimentin. To validate uniform protein loading, the identical blot underwent stripping and reprobing for β-actin. The bar diagram displays the quantitation of corresponding western blots, with the dotted line denoting no significant change, as seen with control antisense (panel D).

respectively, of the total detergent-soluble membrane proteins in normal and OC cells. The values represent mean ± SD from three separate determinants with three replicates ($n = 9$). These results strongly indicate increased RLIP expression in OC cells in contrast to their nonmalignant counterparts (Table 1).

3.2. RLIP-targeting agents and carboplatin reduce the viability of OC cells

In an earlier investigation, we demonstrated the induction of apoptosis in various cultured human malignant cells, encompassing OC, melanoma, breast cancer, prostate cancer, lung cancer, and renal cancer cells, through RLIP depletion using phosphorothioate antisense targeting $nt^{508–528}$ of RLIP. RLIP depletion led to significant regression in established subcutaneous murine B16 melanoma and several other cancers [13, 14, 17–20]. The heightened vulnerability of malignant cells to the cytotoxic effects of RLIP antisense in contrast to immortalized nonmalignant cells was noteworthy; to further examine the impact of suppressing RLIP in OC cells, we utilized RLIP antibodies to inhibit and RLIP antisense for depletion. For a comparative control, the immunoglobulin fraction derived from preimmune serum using Protein-A affinity was utilized. The verification of the RLIP antibodies employed in this study underwent scrutiny through the Ouchterlony double immuno-diffusion assay, ensuring their absence of cross-reactivity with proteins such as P-glycoprotein or multidrug resistance protein [21]. Subjecting cells to preimmune serum or RLIP antibodies (at a final concentration of 40 μg/ml) or scrambled antisense or RLIP antisense (at a final concentration of 10 μg/ml) for 48 h, we observed significant growth inhibitory effects in OC cells treated with RLIP antibodies and RLIP antisense compared with respective controls (Fig. 1B). Conversely, RLIP inhibition or depletion did not manifest noticeable impacts on the growth of nonmalignant HUVEC and HAVSMC cells. We investigated the antiproliferative effects of carboplatin, a commonly used platinum-based drug in OC treatment, on OC cells (OVCAR4, OVCAR8, and MDAH2774) using an MTT assay. Cells underwent treatment with carboplatin at concentrations ranging from 0 to 100 μM for 48 h. Carboplatin-treated cells exhibited a substantial concentration-dependent decrease in viability, whereas non-tumorigenic cells (HUVEC and HAVSMC) showed no discernible growth inhibitory effects. The IC_{50} values (μM) of carboplatin and the percentage of cell survival after RLIP antibody and RLIP antisense treatment for each cell line are presented in the table of Fig. 1B. Consistent results were also obtained with the CCK-8 cell viability assay. To further affirm the impact of RLIP depletion on cell survival and proliferation in OC cells, we assessed their clonogenic potential. The colony-forming assay results demonstrated that RLIP antisense treatment effectively reduced RLIP levels, leading to a reduction in the clonogenicity of OC cells (Fig. 1C).

Table 1. RLIP protein in human normal and OC cells.

	Total crude protein (mg/10^8 cells)	RLIP protein	
		µg/10^8 cells	% of total crude protein
Nonmalignant			
HAVSMC (aorta smooth muscle)	5.48 ± 0.47	11 ± 2	0.20
HUVEC (umbilical endothelial)	5.61 ± 0.52	10 ± 2	0.18
Malignant			
OVCAR4	6.47 ± 0.31	48 ± 4	0.74
OVCAR8	6.93 ± 0.43	49 ± 5	0.71
MDAH2774	8.11 ± 0.37	58 ± 4	0.72

Homogenates were generated from 100 × 10^6 cells cultured in their respective media, and RLIP was extracted from total crude membrane fractions through dinitrophenyl-S-glutathione (DNP-SG) affinity column chromatography. Quantification was carried out using ELISA, with calibration curves established using purified recombinant RLIP. The values represent mean ± SD from three separate determinants with three replicates (n = 9). The normal cell types utilized included HUVEC and HAVSMC. ELISA, enzyme-linked immunosorbent assay.

3.3. RLIP antisense downregulates a cancer signaling pathway in OC cells

A connecting link between OC cell resistance to cisplatin and Akt has been documented [22, 23]. To investigate the impact on crucial intracellular proteins, MDAH2774 cells underwent a 24-h treatment with RLIP antisense and were subjected to western blot analysis (Fig. 1D). In several ovarian tumors, the activation of PI3K/Akt signaling is consistently observed [23]. PI3K acts as a central signaling hub, transmitting mitogenic signals in response to cell membrane receptors such as growth factors and integrins. Remarkably, the administration of RLIP antisense resulted in a notable reduction in PI3K phosphorylation. Additionally, the use of RLIP antisense markedly diminished both the protein levels and phosphorylation of Akt in MDAH2774 cells (Fig. 1D). Crucially, there was no indication of Akt or PI3K phosphorylation in normal HUVEC cells (data not presented), consistent with established knowledge that these proteins exhibit activity in transformed cells [24]. Critical signaling mediators such as PI3K and Akt regulate essential downstream targets linked to apoptosis, proliferation, and the perpetuation of malignant characteristics. Akt activation is correlated with the suppression of E-cadherin expression [25]. The reduction in E-cadherin, a well-established marker of the typical epithelial phenotype, is associated with the "Epithelial Mesenchymal Transition (EMT)" and the acquisition of an aggressive phenotype in malignancies [25–28]. PI3K activation hampers the expression of proapoptotic Bim/Bax, promoting the survival and growth of cancer cells [27]. Resistance to mTOR inhibition has been associated with elevated levels of antiapoptotic Bcl2 and CDK4 [28]. Notably, after depleting RLIP using antisense oligonucleotides, a marked increase in the pro-differentiation protein E-cadherin and the proapoptotic protein Bax was evident. In contrast, the antiapoptotic proteins Bcl2, cyclin B1, and CDK4 underwent significant downregulation in MDAH2774 cells. These observations strongly imply a substantial impact on key mediators within the PI3K/Akt signaling axis in OC due to the reduction of RLIP (Fig. 1D, inset).

3.4. Effect of RLIP depletion on apoptosis

To further illustrate the influence of diminishing RLIP on proliferative capacity, we investigated apoptosis in OC cells (OVCAR4, OVCAR8, and MDAH2774). Verification of RLIP reduction was achieved through western blot analysis of cells subjected to RLIP antisense treatment (Fig. 2A). Moreover, the colony-forming assay exhibited significant suppression of clonogenic potential (Fig. 1C). RLIP depletion exerts *in vitro* anti-migratory and anti-invasive effects on OC cells; the metastatic cascade involves complex phases of cell migration and invasion, facilitating the spread of tumor cells to distant organs from their point of origin. To assess the impact of RLIP reduction on migration, we conducted a scratch wound healing assay using MDAH2774 and OVCAR8 cells treated with either scrambled or RLIP antisense (final concentration of 10 µg/ml). At 12 and 24 h, the assay revealed a notable impediment in the migratory capability of OC cells with RLIP antisense treatment (Fig. 2B). Subsequent to this, we investigated the impact of RLIP antisense treatment (final concentration of 10 µg/ml) on the invasion of MDAH2774 OC cells within 24 h, utilizing Matrigel® invasion chambers. As displayed in Fig. 2C, crystal violet stain revealed a significant reduction in the count of invading cells in RLIP antisense-treated cells compared with the control. These outcomes imply that RLIP depletion hinders the *in vitro* invasive capability of OC cells (Fig. 2C). Encouraged by these findings, we proceeded to evaluate the potential of RLIP depletion/inhibition alongside carboplatin in inducing regression in xenografts of OC MDAH2774 cell lines.

3.5. Antineoplastic effects of RLIP depletion/inhibition and carboplatin

We evaluated the combined cytotoxic impact of drug combinations in three OC cell lines (MDAH2774, OVCAR4, and OVCAR8), and the outcomes are depicted for a single fixed-dose combination (Fig. 3A). The Rab + carbo combination exhibited a supra-additive effect, along with the Rab + RAS + carbo combination, while RAS + carbo demonstrated either an additive or sub-additive effect. Analyses following the Chou–Talalay method were conducted to evaluate synergy by employing different combinations of dose effects for the three agents. The results confirmed synergy for the Rab + RAS + carbo combination, while indicating additive effects for Rab + carbo and RAS + carbo combinations.

These *in vitro* predictions were subsequently validated in a nude mouse xenograft model using the OC MDAH2774 cell line. The utilization of human xenografts in mice is prevalent for examining metastasis patterns and *in vivo* reactions

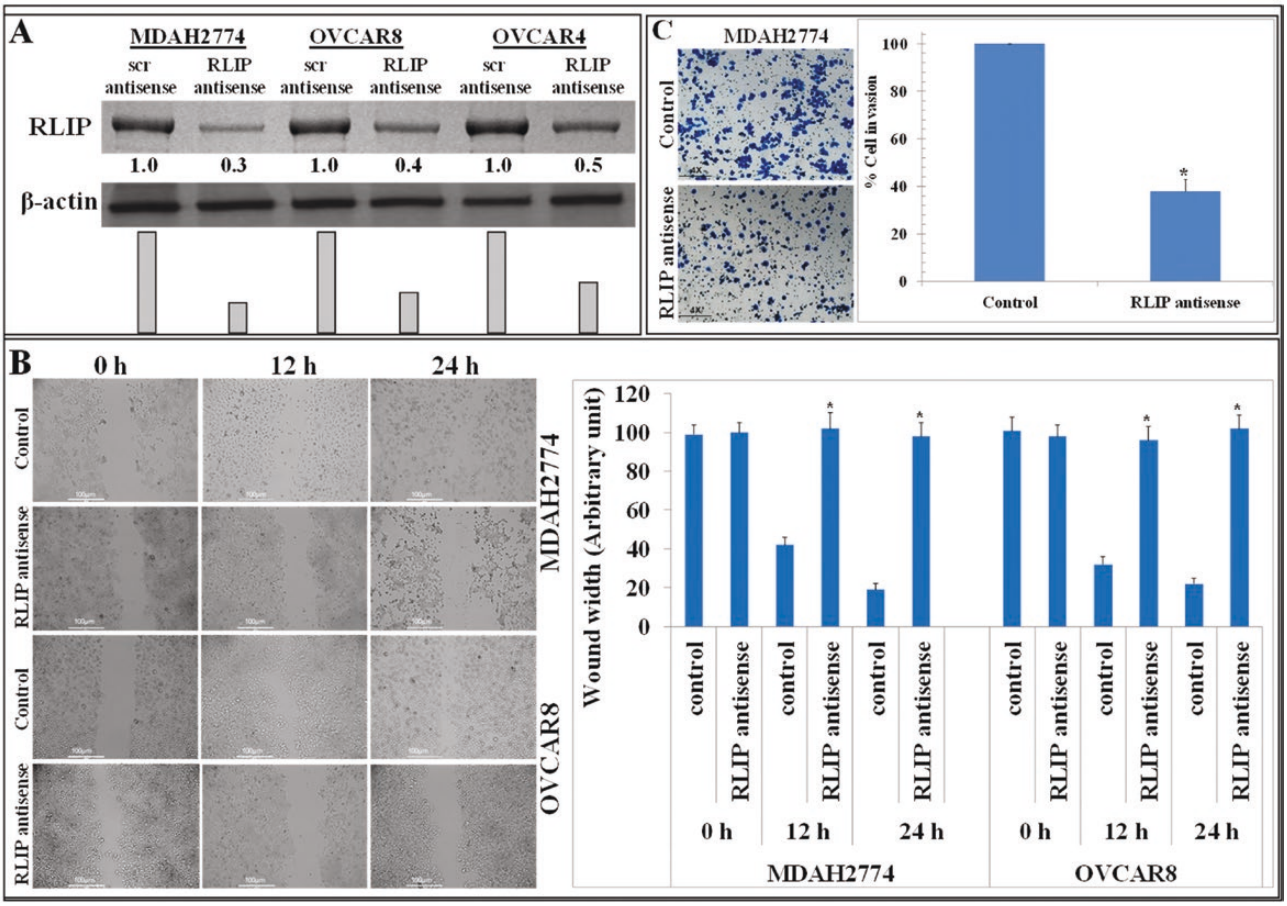

Figure 2 Impact of RLIP antisense on both RLIP expression and apoptosis. Assessment of RLIP depletion involved western blot analyses, utilizing 100 μg of OC (OVCAR4, MDAH2774, and OVCAR8) crude membrane fractions 24-h post-treatment. Cells were treated with either scrambled or RLIP antisense (10 μg/ml final concentration). Quantification utilized Innotech Alpha Imager HP scanning densitometry, with β-actin as the internal control. The numbers below the blots indicate the fold change in protein levels compared with the control, determined through densitometry. The experiment was conducted thrice, and the displayed image represents one trial. The densitometry analysis bar graph is illustrated (panel A). Effects of RLIP antisense on the migration and invasion of OC cell lines. Culturing MDAH2774 and OVCAR8 OC cells to 90% confluence in cell culture dishes, a scratch or wound was introduced in each dish. Subsequently, the cells underwent a 24-h treatment with either scrambled or RLIP antisense (10 μg/ml final concentration). Images were captured at each time point for both control and treatment groups, and the wound width was measured across the scratch in three replicate experiments, with the results quantified and presented. Statistical significance was determined by Student's *t*-test (**P* < .02) compared with respective controls (panel B). MDAH2774 cells were placed in the upper chamber of transwell inserts (8 μm pore size) in serum-free medium and treated with either scrambled or RLIP antisense (10 μg/ml final concentration) for 24 h. The invaded cells were fixed with 4% paraformaldehyde and stained with 0.2% crystal violet. Subsequently, invasive cells were photographed under a light microscope at 200× magnification. The quantification of invaded cells in RLIP antisense-treated cells is presented after normalization to the percentage of invaded cells in the control. Statistically significant differences (**P* < .02) compared with the controls were determined by Student's *t*-test (panel C).

to drug combinations. The subcutaneous inoculation route enables straightforward monitoring of tumor size, providing insights into the response to experimental intervention in the mouse. Animals hosting established MDAH2774 tumors implanted subcutaneously (~35 mm^2) were administered intraperitoneal injections of 100 μl PBS containing Rab (4 mg/kg b.w.), RAS (4 mg/kg b.w.), carbo (20 mg/kg b.w.), or various combinations, once a week for 8 weeks (Figs 3 and 4). The Rab + carbo and RAS + carbo combinations exhibited enhanced effectiveness in tumor regression compared with individual drug treatments. Notably, animals treated with Rab or RAS demonstrated quicker responses than those treated with carboplatin alone. Remarkably, the combined treatment involving all three agents led to the most rapid remission (Fig. 3B and C). Tumor weights on day 56, post-initiation of treatment, reflected a substantial reduction in tumor volume (Fig. 3D). The mice in each treatment group displayed comparable average weight gain, affirming the safety and absence of adverse effects for all interventions (Fig. 3E). Western blot analyses of tumor homogenates confirmed the effectiveness of RLIP antisense in reducing tumors *in vivo* (Fig. 3F).

Significantly, all rodents experienced a reduction in tumor implants following RLIP depletion and inhibition, without any detectable adverse effects or influences on weight gain. Macroscopic observation revealed an absence of cancer spreading to other organs in all experimental groups. Furthermore, the introduction of carboplatin led to a noteworthy additional decrease in tumor regression. These findings suggest that RLIP blockade likely involves membrane transporters, and the addition of carboplatin enhances cytotoxicity. Furthermore, these results anticipate that RLIP antibodies should exhibit at least equal antitumor efficacy as antisense, assuming the antiapoptotic activity of RLIP depends on its transport function. The combination of a mercapturic

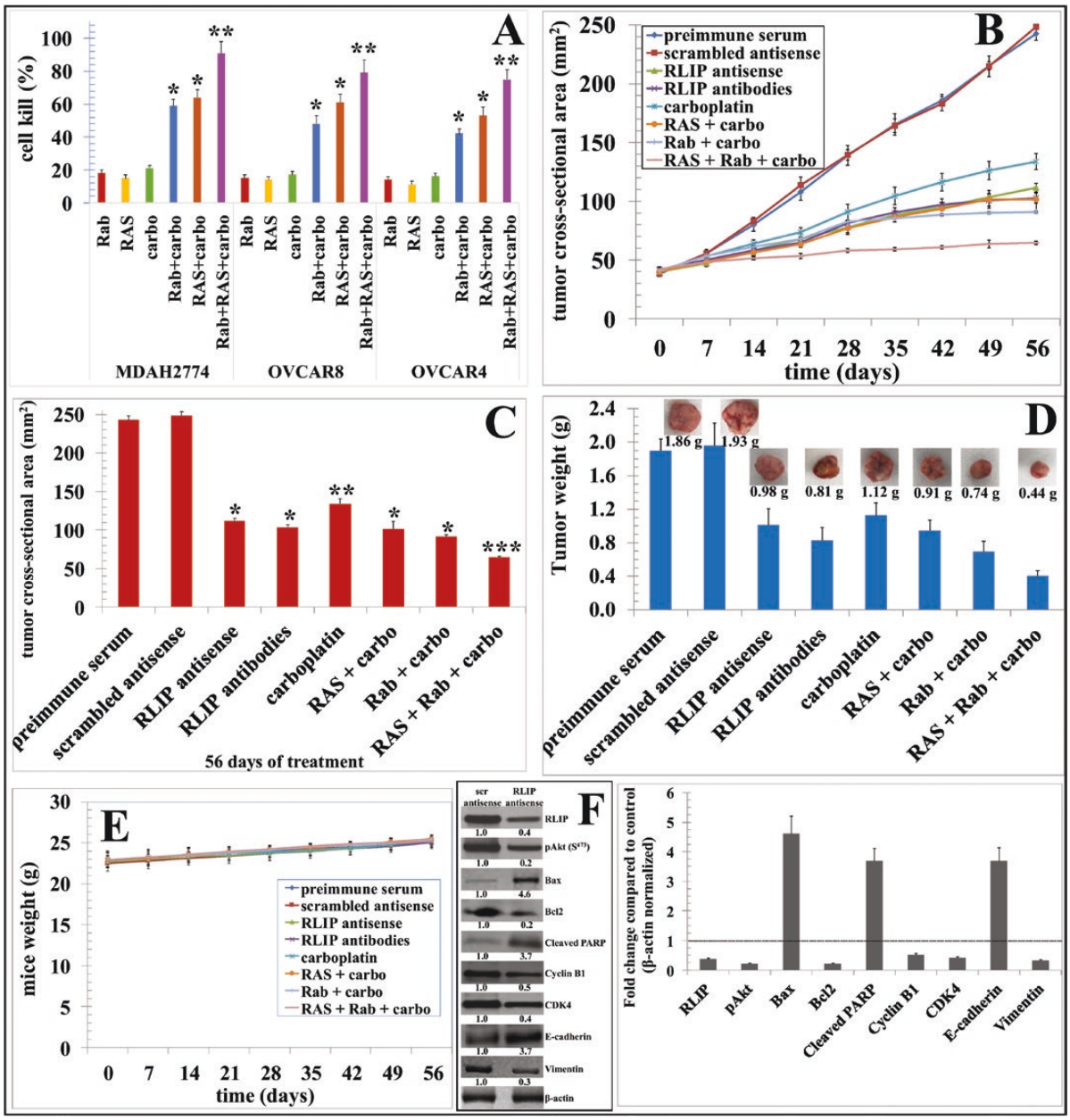

Figure 3 Comparison of antineoplastic effects of RLIP antibodies, RLIP antisense, and carboplatin on OC cells. Assessment of *in vitro* cytotoxic interactions involving RLIP antibodies, RLIP antisense, and carboplatin was conducted through MTT cytotoxicity assays, with absorbance values used to calculate cytotoxic effects. Cells were subjected to individual or combined treatments with RLIP antibodies (10 μg/ml), RLIP antisense (2 μg/ml), and carboplatin (10 μM) for 48 h prior to the MTT assay. Three separate experiments, each with four replicates, were performed ($n = 12$). *$P < .03$ compared with single drug treatment; **$P < .01$ three drugs combination treatment compared with single drug treatment (panel A). *In vivo* antineoplastic interactions of RLIP antisense, RLIP antibodies, and carboplatin were investigated in xenografts of human ovarian MDAH2774 cells. Athymic nude mice were implanted with 1×10^6 MDAH2774 cells and treated with different interventions: (i) preimmune serum, (ii) scrambled antisense, (iii) RLIP antisense 4 mg/kg b.w., (iv) RLIP antibodies 4 mg/kg b.w., (v) carboplatin 20 mg/kg b.w., (vi) RLIP antisense + carboplatin, (vii) RLIP antibodies + carboplatin, and (viii) RLIP antibodies + RLIP antisense + carboplatin. Tumor growth was notably slower in mice receiving RLIP antibodies, RLIP antisense, or carboplatin alone, as well as their combinations, compared with respective control treatment mice (panel B). A comparison of tumor cross-sectional area (mm^2) at the conclusion of the study on day 56 is depicted. *$P < .02$ compared with control treatment; **$P < .03$ compared with control treatment; ***$P < .01$ drugs combination treatment compared with control treatment (panel C). The average wet weight of tumors on day 56 was notably lower in groups treated with RLIP antibodies, RLIP antisense, and carboplatin alone, as well as their combinations, in comparison to control treatment mice (controls: 1.86 g; 1.93 g versus experimental: 0.98, 0.81, 1.12, 0.91, 0.74, and 0.44 g, respectively (panel D). Mice subjected to RLIP antisense, RLIP antibodies, or carboplatin did not display indications of stress or evident toxicity, such as compromised movement, posture irregularities, digestive disturbances, or localized redness or swelling. No notable variations in the initial and concluding body weights were observed between the mice treated with control and experimental substances (panel E). Examining the influence of cancer signaling pathways in excised tumors from OC xenografts post-antisense treatment involved analyzing signaling proteins through western blot analysis in MDAH2774 human ovarian tumor tissue lysates from both RLIP antisense and scrambled antisense treated groups. β-Actin served as the loading control, and the numbers below the blots represent the fold change in protein levels compared with the control, determined by densitometry. The dotted line indicates no substantial change, as observed with scrambled antisense (panel F). These findings offer crucial *in vivo* evidence regarding the growth-inhibiting effects of agents targeting RLIP, including RLIP antibodies and RLIP antisense, as well as carboplatin in OC. The values presented in both the line graph and bar graph represent the mean ± SD from five mice in each respective group. RLIP antisense is abbreviated as RAS, RLIP antibodies as Rab, and carboplatin as carbo.

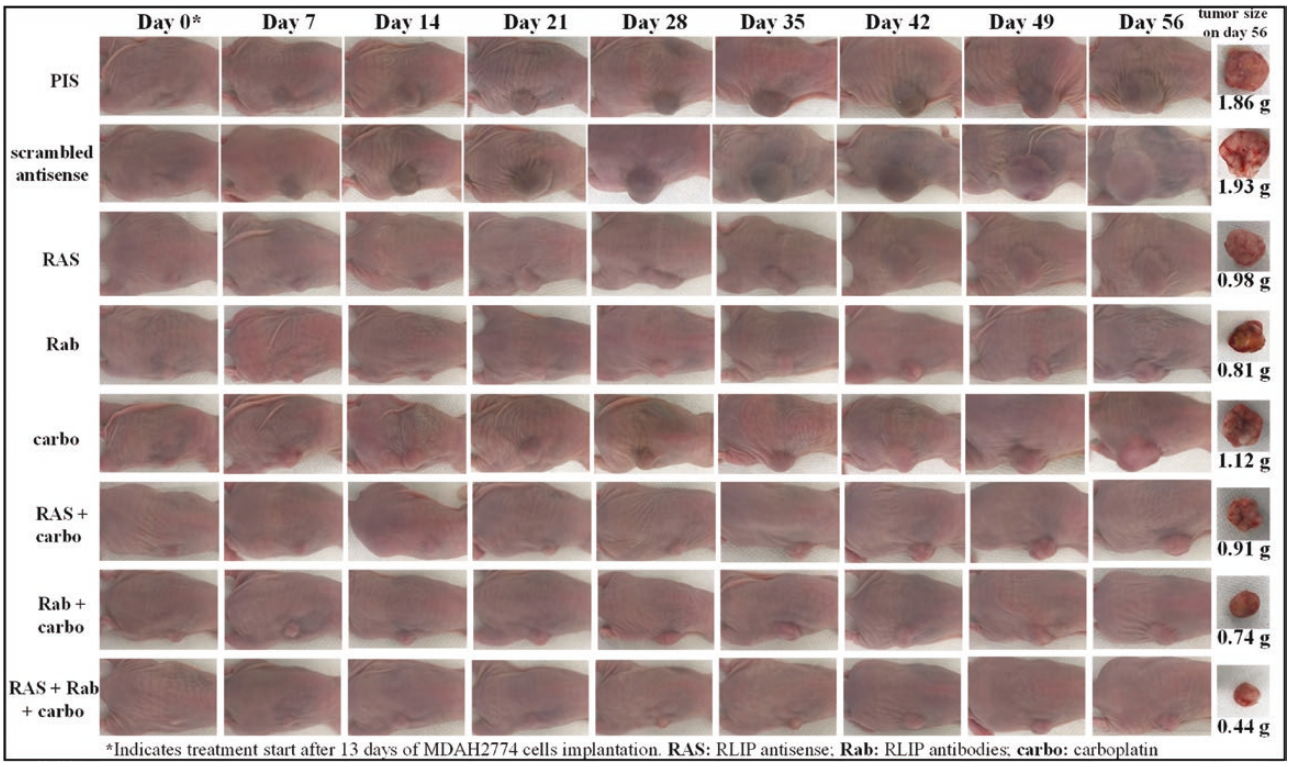

Figure 4 Impact of RLIP antibodies, RLIP antisense, and carboplatin on the size of human OC (MDAH2774) subcutaneously implanted in nude mice. Female nude athymic *nu/nu* mice procured from The Jackson Laboratory, Bar Harbor, ME, underwent a 1-week acclimatization period before the commencement of the experiment. All animal procedures adhered to an approved protocol by the Institutional Animal Care and Use Committee (IACUC #22011). A total of forty 10-week-old mice were divided into eight groups, each consisting of five animals, and received diverse treatments: (i) scrambled antisense, (ii) RLIP antisense 4 mg/kg b.w., (iii) preimmune serum, (iv) RLIP antibodies 4 mg/kg b.w., (v) carboplatin 20 mg/kg b.w., (vi) RLIP antisense + carboplatin, (vii) RLIP antibodies + carboplatin, and (viii) RLIP antibodies + RLIP antisense + carboplatin. Subcutaneous injections of 1×10^6 MDAH2774 cell suspensions in 100 µl of PBS were administered into one flank of all 40 animals. Daily evaluations were carried out to monitor tumor growth, and upon achieving a cross-sectional area of ~35 mm^2 (13 days later), animals underwent randomization into treatment groups as indicated in the figure. The treatment regimen involved weekly intraperitoneal injections of 100 µl doses for 8 weeks, delivering RLIP antisense, RLIP antibodies, or carboplatin alone, along with their various combinations. Control groups received 100 µl of preimmune serum and scrambled antisense. Tumor dimensions were measured using calipers in two dimensions, and body weights were recorded. Photographs of the animals were taken on days 1, 7, 14, 21, 28, 35, 42, 49, and 56 after treatment, encompassing all groups. Additionally, tumor images were captured on day 56 post-treatment.

acid pathway (MAP) inhibitor and the chemotherapeutic agent carboplatin could potentially represent one of the most effective treatments for OC.

3.6. Tumor growth inhibition is associated with the inhibition of cancer signaling pathways

To further explore the molecular alterations linked to the inhibition of tumor growth, we utilized western blot analysis on lysates extracted from ovarian tumor tissues, comparing those subjected to RLIP antisense treatment with control tumors. The analysis concentrated on vital components of the PI3K/Akt signaling pathway and other noteworthy downstream signal transducers. Our findings revealed a significant decrease in the phosphorylation of PI3K and Akt in tumors treated with RLIP antisense. We examined the expression of key regulators, including proapoptotic Bax, E-cadherin, cyclin B1, and CDK4, within the tumors, all playing crucial roles in influencing cancer growth, differentiation, and apoptosis. In the tumor tissue lysates from mice treated with RLIP antisense, vimentin, cyclin B1, and CDK4 levels exhibited a notable decrease compared with controls, while the proapoptotic protein Bax and the tumor suppressor E-cadherin displayed significantly elevated levels (Fig. 3F). These results highlight the correlation between impeding tumor growth and suppressing the cancer signaling pathway.

Conducting immune-histochemical analysis on ovarian tumor sections treated with RLIP antisense, we observed reduced levels of RLIP, the mesenchymal marker vimentin, the proliferation indicator Ki67, and the angiogenesis marker CD31. In contrast, enhanced levels of the epithelial differentiation marker E-cadherin were evident (Fig. 5). These findings affirm our *in vitro* observations, emphasizing that RLIP depletion substantially impedes cell proliferation and promotes apoptosis in OC. The compelling discoveries not only validate RLIP as a promising therapeutic target, but also strongly support our conceptual model of RLIP, illustrating its protective role against stress through transport activity [14].

These findings distinctly reveal that RLIP antibodies, in isolation, exhibit antineoplastic efficacy in xenograft models of human OC, comparable to a fixed concentration of carboplatin. The absence of an incremental impact of carboplatin on the effectiveness of RLIP antibodies alone implies that carboplatin's apoptotic effects might involve competitive inhibition of physiological glutathione-derived species, such as glutathione-conjugate of 4-hydroxynonenal (4HNE-SG), by disrupting their transport facilitated by RLIP. According to this model, an additional impact of carboplatin

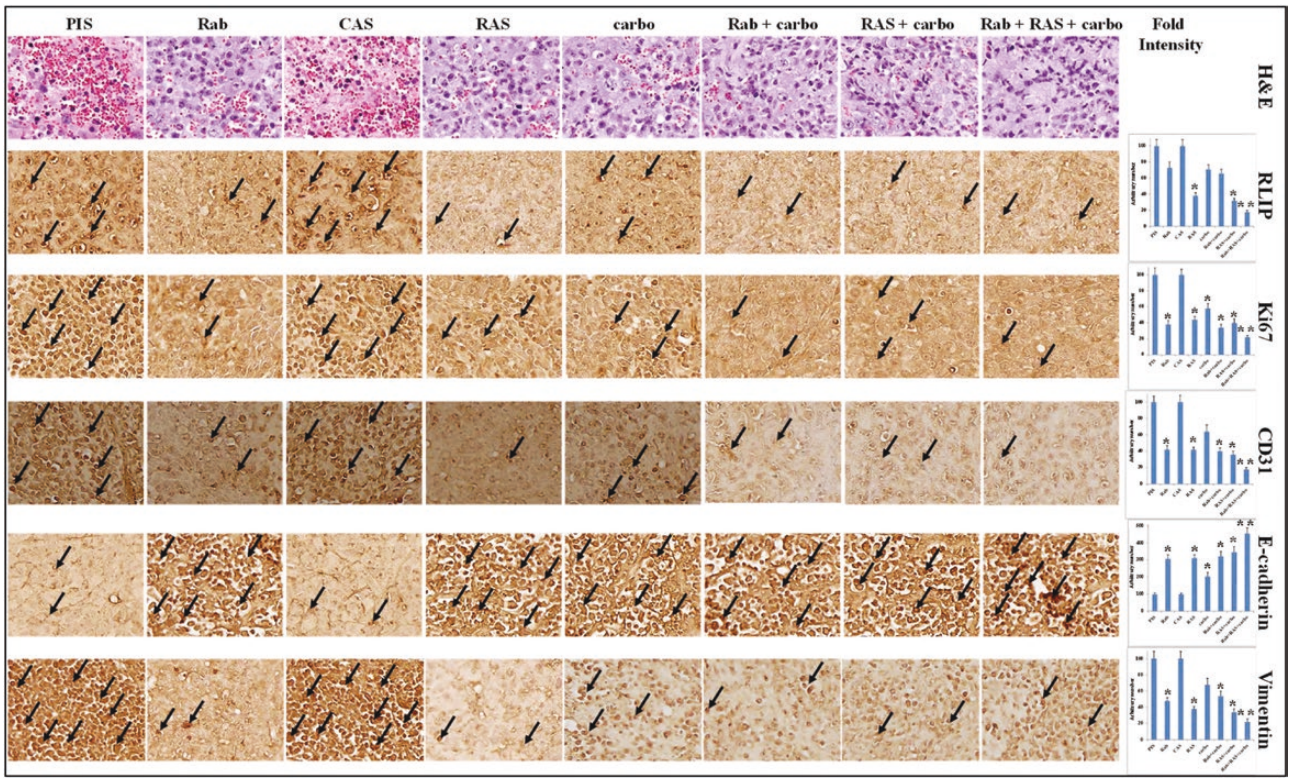

Figure 5 Immunohistochemical analyses, indicating the inhibition of RLIP restrains the expression of proliferation and angiogenesis markers in MDAH2774 ovarian xenograft tumors. Histopathological assessments were performed on tumor sections obtained from both control and experimentally treated nude mice harboring OC. The experimental findings include sections stained with H&E and IHC analyses, assessing the expression of RLIP, CD31, E-cadherin, Ki67, and vimentin. Statistical significance, determined using a two-tailed Student's *t*-test, demonstrated $^{*}P < .04$ and $^{**}P < .02$ for RLIP-targeting agents compared with the controls. Immunoreactivity is evident as a dark brown stain, whereas nonreactive areas display only the background color. Photomicrographs at 40× magnification were captured using an Olympus DP 72 microscope. The staining percentage was determined by assessing positive immunoreactivity per unit area, and the Pro Plus software was employed for digital image analysis to quantify the intensity of antigen staining. Arrows represent the area for positive staining for an antigen. The graphs depict the mean ± standard error ($n = 5$), with abbreviations such as PIS for preimmune serum, Rab for RLIP antibodies, CAS for scrambled antisense, RAS for RLIP antisense, and carbo for carboplatin.

is not expected when RLIP is restrained. The sensitive influence of RLIP antisense or RLIP antibodies when combined with carboplatin could be linked to distinct yet interconnected binding sites on RLIP for GS–E and natural product toxins. Consequently, the simultaneous presence of RLIP antibodies, RLIP antisense, and carboplatin might enhance the inhibition of efflux for physiological ligands (GS–E derived from lipid hydroperoxides).

4. Discussion

Epithelial ovarian cancer stands as the most formidable gynecological malignancy. The PI3K/Akt cascade assumes a crucial role in the progression, dissemination, and metastasis of various human cancers. Genomic investigations suggest a higher frequency of mutational alterations in this OC-related pathway compared with other malignancies [5, 29]. Existing evidence also points to the involvement of PI3K/Akt signaling in conferring chemoresistance and predicting a poor prognosis in OC. Despite multiple clinical trials with PI3K/Akt inhibitors, their efficacy remains suboptimal due to the challenges posed by frequent mutations, disease heterogeneity, complexity, toxicity, and the emergence of chemoresistance phenotypes [30, 31]. Surgery and chemotherapy, utilizing carboplatin and paclitaxel, have long been established as the foundational approach for primary OC management. However, even with optimal surgery and appropriate first-line chemotherapy, approximately 75% of epithelial OC patients experience disease relapse [32–35]. Consequently, there is an urgent demand for the development of novel drug candidates to address this pressing need in OC prevention. The RLIP MAP transporter, recognized as a stress-protective protein and functioning as an Ral effector in clathrin-dependent endocytosis, displays heightened expression in OC and plays a pivotal role in fostering resistance to radiation and chemotherapy. Through diverse mechanisms, including enhanced detoxification of lipid peroxidation products and modulation of intracellular signaling pathways [10, 17–20], RLIP actively maintains the survival and proliferation of cancer cells. By promoting the accumulation of endogenously generated GS–E, RLIP induces apoptosis in cancer cells.

In our ongoing research, we demonstrate that intraperitoneal delivery of RLIP antisense or RLIP antibodies results in sustained regression of xenograft tumors in nude mice with OC. These findings emphasize that RLIP is a vital survival protein for OC cells, where its depletion or inhibition leads to the retreat of human OC xenografts without apparent harm to animals. The consistent outcomes achieved by both RLIP antibodies and RLIP antisense support the idea that RLIP's antiapoptotic and stress-protective

effects are primarily linked to its transport activity [14]. Despite being mainly located in the cytosol, RLIP's transport function enables it to associate with the membrane as well [36]. Our results establish RLIP as a unique target for anticancer interventions, functioning both as a versatile and efficient multidrug transporter and an antiapoptotic protein crucial for the survival of cancer cells. RLIP provides a survival advantage to cancer cells by effectively transporting glutathione conjugates of endogenous proapoptotic molecules (e.g. 4HNE) and chemotherapeutic drugs. Notably, 4HNE, the predominant reactive alkenal resulting from lipid peroxidation, serves as a toxic endogenous alkylating agent [37, 38]. The modulation of cellular 4HNE levels influences proliferation, with lower levels promoting increased proliferation and higher concentrations triggering differentiation, apoptosis, and necrosis [39]. Demonstrated by a substantial reduction (approximately 80%) in GS–E transport activity in RLIP homozygous knockout mice ($RLIP^{-/-}$) tissues, there is apparent increased sensitivity to GS–E-generating stresses like X-irradiation and oxidant chemicals [12]. Swift reduction of RLIP through small interfering RNA (siRNA) or antisense, or the hindrance of transport using antibodies directed at cell-surface epitopes, initiates selective apoptosis in cancer cells while sparing nonmalignant cells [13].

RLIP antibodies exhibit greater efficacy compared with carboplatin alone, emphasizing the significance of RLIP as an anticancer target. This suggests that carboplatin-induced apoptosis might involve competitive inhibition of the transport of physiological substrates, such as glutathione-conjugate of 4-hydroxynonenal (GS-HNE) derived from oxidative metabolism, as evidenced in transport studies utilizing both artificial and cell-membrane-derived liposomes [7]. The heightened effectiveness observed with the three-drug combination implies potential synergy in inhibiting not only RLIP but also other ABC-family transporters. Combining RLIP depletion or inhibition with carboplatin demonstrates significant and synergistic effects in OC. Our recent results affirm that RLIP depletion or inhibition leads to the regression of OC tumors, particularly when combined with carboplatin. Additionally, our investigations suggest that agents targeting RLIP impede the oncogenic potential of OC cells and improve chemosensitivity by targeting the PI3K/Akt axis.

5. Conclusions

OC frequently appears at advanced stages, characterized by extensive metastasis throughout the peritoneal cavity. The findings presented in this study highlight that inhibiting or depleting RLIP exerts significant antineoplastic effects in OC. This underscores the crucial role of GS–E and xenobiotic transporters in the hierarchy of stress defense mechanisms essential for the survival of cancer cells. *In vivo* studies further demonstrate that the combined administration of therapy (RLIP antisense + RLIP antibodies + carboplatin) synergistically and safely inhibits the growth of MDAH2774 tumors. In summary, the co-delivery approach of RLIP-targeting agents and carboplatin holds promise for clinical application as a treatment for OC.

6. Clinical impact

OC stands as the most lethal gynecological cancer globally, and its asymptomatic early stage coupled with a lack of sensitive screening methods results in approximately 70% of patients being diagnosed at an advanced stage. Despite the emergence of novel anticancer drugs like paclitaxel and carboplatin, there remains a lack of consensus on their efficacy. Current evidence suggests that these drugs do not significantly improve overall survival or reduce side effects in treating platinum-sensitive OC. Major challenges arise from acquired resistance and adverse side effects to traditional platinum-based chemotherapy, underscoring the necessity for cancer-specific defect-targeting anticancer drugs with greater selectivity. Compounds targeting RLIP trigger apoptosis via both intrinsic and extrinsic pathways, leading to G2 cell cycle arrest mediated by cyclin B1 in OC cells. These findings shed light on how inhibiting or depleting RLIP may contribute to preventing and treating platinum-resistant OC. Therefore, exploring therapeutic drugs targeting the PI3K/Akt signaling pathway presents a promising avenue for OC treatment. In conclusion, our data provide potential targets for therapeutic interventions in OC patients.

Highlights

- Utilizing human cell line xenografts proves invaluable for delving into cancer biology and gauging treatment responses.
- Accelerating the transition from *in vitro* studies to *in vivo* testing requires the characterization of growth conditions in mice.
- Cancer development is influenced by oxidative stress, fostering mutagenesis and abnormal activation of signaling pathways crucial for tumor growth and progression.
- Treatment with RLIP antisense reduces levels of Bcl2, RLIP, CDK4, cyclin B1, pAKT, and vimentin, while elevating levels of Bax and E-cadherin.
- Substances that inhibit/deplete RLIP or induce its downregulation act as broad-spectrum OC therapeutics, irrespective of frequent alterations in signaling pathways.

Acknowledgments

Our appreciation extends to the team at the Pathology Cores and the Animal Research Centre for their crucial assistance. Special acknowledgment goes to Erin Keebaugh for her editorial contributions to this manuscript. We genuinely recognize Dr Ravi Salgia for endorsing our study and serving as the Professor and Chair of the Department of Medical Oncology at City of Hope.

Author contributions

S.S.S. and M.K. contributed to data collection and manuscript writing. S.K.R. contributed to data collection, literature search, and statistical analysis. P.G. and E.W. contributed to data analysis and interpretation. D.H. reviewed and edited the manuscript. P.K. and S.A. contributed to discussion and reviewed and edited the manuscript. A.M. and R.S. contributed to data interpretation.

Participation consent and ethics approval

Human participants were not part of this study. The research involving animals followed IACUC protocol #22011, which

gained approval from the City of Hope Animal Care and Ethics Committee.

Conflict of interest statement: None declared.

Funding

The project received funding from the National Cancer Institute of the National Institutes of Health (P30CA33572) and the United States Department of Defense (W81XWH-22-1-0331 and HT9425-23-1-0581). Furthermore, appreciation is expressed for the financial backing provided by City of Hope's Beckman Research Institute.

Data availability

The corresponding author is available to share any data generated or analyzed in the course of the present study upon request.

References

1. Siegel RL, Giaquinto AN, Jemal A. Cancer statistics. *CA Cancer J Clin* 2024;**74**:12–49.
2. Ortiz M, Wabel E, Mitchell K *et al*. Mechanisms of chemotherapy resistance in ovarian cancer. *Cancer Drug Resist* 2022;**5**:304–16.
3. Zhou Y, Guo W. Efficacy and safety of paclitaxel and carboplatin for platinum-sensitive ovarian cancer: a systematic review and meta-analysis. *J Clin Phar Ther* 2023;**2023**:1–8.
4. Agarwal R, Kaye SB. Ovarian cancer: strategies for overcoming resistance to chemotherapy. *Nat Rev Cancer* 2003;**3**:502–16.
5. Mabuchi S, Kuroda H, Takahashi R *et al*. The PI3K/AKT/mTOR pathway as a therapeutic target in ovarian cancer. *Gynecol Oncol* 2015;**137**:173–9.
6. Pokhriyal R, Hariprasad R, Kumar L *et al*. Chemotherapy resistance in advanced ovarian cancer patients. *Biomark Cancer* 2019;**11**:1179299X19860815.
7. Awasthi S, Singhal SS, Srivastava SK *et al*. Adenosine triphosphate-dependent transport of doxorubicin, daunomycin, and vinblastine in human tissues by a mechanism distinct from the P-glycoprotein. *J Clin Invest* 1994;**93**:958–65.
8. Awasthi S, Cheng J, Singhal SS *et al*. Novel function of human RLIP76: ATP-dependent transport of glutathione conjugates and doxorubicin. *Biochemistry* 2000;**39**:9327–34.
9. Sharma R, Singhal SS, Wickramarachchi D *et al*. RLIP76 (RALBP1) mediated transport of leukotriene C4 (LTC4) in cancer cells: implications in drug-resistance. *Int J Cancer* 2004;**112**:934–42.
10. Awasthi S, Singhal SS, Sharma R *et al*. Transport of glutathione conjugates and chemotherapeutic drugs by RLIP76 (RALBP1): a novel link between G-protein and tyrosine kinase signaling and drug resistance. *Int J Cancer* 2003;**106**:635–46.
11. Stuckler D, Singhal J, Singhal SS *et al*. RLIP76 transports vinorelbine and mediates drug resistance in non-small cell lung cancer. *Cancer Res* 2005;**65**:991–8.
12. Awasthi S, Singhal SS, Yadav S *et al*. RLIP76 is a major determinant of radiation sensitivity. *Cancer Res* 2005;**65**:6022–8.
13. Singhal SS, Awasthi YC, Awasthi S. Regression of melanoma in a murine model by RLIP76 depletion. *Cancer Res* 2006;**66**:2354–60.
14. Ramisetty S *et al*. Regression of ovarian cancer xenografts by depleting or inhibiting RLIP. *Biochem Pharmacol* 2023 (PMID: 37804871).
15. Chou TC, Motzer RJ, Tong Y *et al*. Computerized quantitation of synergism and antagonism of taxol, topotecan, and cisplatin against human teratocarcinoma cell growth: a rational approach to clinical protocol design. *J Natl Cancer Inst* 1994;**86**:1517–24.
16. Singhal SS, Yadav S, Drake K *et al*. Hsf-1 and POB1 induce drug-sensitivity and apoptosis by inhibiting Ralbp1. *J Biol Chem* 2008;**283**:19714–29.
17. Awasthi S, Singhal SS, Awasthi YC *et al*. RLIP76 and cancer. *Clin Cancer Res* 2008;**14**:4372–7.
18. Singhal SS, Wickramarachchi D, Yadav S *et al*. Glutathione-conjugate transport by RLIP76 is required for clathrin-dependent endocytosis and chemical carcinogenesis. *Mol Cancer Ther* 2011;**10**:16–28.
19. Lee S, Wurtzel JGT, Singhal SS *et al*. RALBP1/RLIP76 depletion in mice suppresses tumor growth by inhibiting tumor neovascularization. *Cancer Res* 2012;**72**:5165–73.
20. Singhal J, Chikara S, Horne D *et al*. Targeting RLIP with CRISPR/Cas9 controls tumor growth. *Carcinogenesis* 2021;**42**:48–57.
21. Singhal SS, Singhal J, Sharma R *et al*. Role of RLIP76 in lung cancer doxorubicin resistance: the ATPase activity of RLIP76 correlates with doxorubicin and 4-hydroxynonenal resistance in lung cancer cells. *Int J Oncol* 2003;**22**:365–75.
22. Abedini MR, Muller EJ, Bergeron R *et al*. Akt modulates cisplatin-induced, p53-dependent ubiquitination of FLICE-like inhibitory protein, promoting chemoresistance in human ovarian cancer cells. *Oncogene* 2010;**29**:11–25.
23. Musa F, Schneider R. Targeting ovarian cancer through the PI3K/AKT/mTOR pathway. *Transl Cancer Res* 2015;**4**:97–106.
24. Chen X, Thakkar H, Tyan F *et al*. Constitutively active Akt regulates TRAIL sensitivity in prostate cancer. *Oncogene* 2001;**20**:6073–83.
25. Julien S, Puig I, Caretti E *et al*. NF-kappaB activation by Akt upregulates Snail expression, inducing epithelium mesenchyme transition in cancer. *Oncogene* 2007;**26**:7445–56.
26. Karayiannakis AJ, Syrigos KN, Chatzigianni E *et al*. Aberrant E-cadherin expression in human pancreatic cancer associates with loss of differentiation and advanced stage. *Anticancer Res* 1998;**18**:4177–80.
27. Sugatani T, Hruska KA. Akt1/Akt2 and mTOR/Bim roles in osteoclast differentiation and survival, with Akt being dispensable for survival in isolated osteoclast precursors. *J Biol Chem* 2005;**280**:3583–9.
28. Aguirre D, Boya P, Bellet D *et al*. Bcl-2 and CCND1/CDK4 expression predict mTOR inhibitor effects in human ovarian carcinoma. *Apoptosis* 2004;**9**:797–805.
29. Matulonis UA. Management of newly diagnosed or recurrent ovarian cancer. *Clin Adv Hematol Oncol* 2018;**16**:426–37.
30. Huang J, Zhang L, Greshock J *et al*. Frequent genetic abnormalities in the PI3K/AKT pathway predict patient outcome in primary ovarian cancer. *Genes Chromosomes Cancer* 2011;**50**:606–18.
31. Carden CP, Stewart A, Thavasu P *et al*. PI3 kinase signaling associates with chemoresistance in advanced ovarian cancer. *Mol Cancer Ther* 2012;**11**:1609–17.
32. Au KK, Josahkian JA, Francis J-A *et al*. Biomarkers in ovarian cancer prognosis. *Future Oncol* 2015;**11**:3187–95.
33. Pignata S, Cecere SC, Du Bois A *et al*. Treatment of recurrent ovarian cancer. *Ann Oncol* 2017;**28**:viii51–6.
34. Ledermann JA. Front-line therapy of advanced ovarian cancer: new approaches. *Ann Oncol* 2017;**28**:viii46–50.
35. Patra B, Lateef MA, Brodeur MN *et al*. Carboplatin sensitivity in epithelial ovarian cancer cell lines: impact of model systems. *PLoS One* 2020;**15**:e0244549.
36. Yadav S, Singhal SS, Singhal J *et al*. Identification of membrane anchoring domains of RLIP76 using deletion mutants analyses. *Biochemistry* 2004;**43**:16243–53.
37. Awasthi YC, Yang Y, Tiwari NK *et al*. Regulation of 4-hydroxynonenal mediated signaling by glutathione S-transferases. *Free Radic Biol Med* 2004;**37**:607–19.
38. Esterbauer H, Schaur RJ, Zollner H. Chemistry and biochemistry of 4-hydroxynonenal, malonaldehyde and related aldehydes. *Free Radic Biol Med* 1991;**11**:81–128.
39. Sharma R, Brown D, Awasthi S *et al*. Transfection with 4-hydroxynonenal-metabolizing glutathione S-transferase isozymes leads to phenotypic transformation and immortalization of adherent cells. *Eur J Biochem* 2004;**271**:1690–701.